A remark on the seismic resolution function for the homogeneous elastic isotropic case

Bobby Hak, Delft University of Technology, and Wim A. Mulder, Shell International Exploration and Production B.V.*

SUMMARY

We examine the resolution function or hessian for a point scatterer in a homogeneous isotropic elastic background. A suitable approximate hessian will improve the efficiency of an elastic migration code. Isotropic elasticity requires three model parameters. Migration of recorded data will mix contributions from perturbations in these parameters. The hessian can be interpreted as the migration result of data generated by a point scatterer. This involves 3×3 migration images. The standard choice of density, P-, and S-impedance provides some decoupling between model parameters, that is, a density perturbation produces the strongest amplitude in the density migration image, and so on. If we want to use the inverse of the block-diagonal part of the hessian as a preconditioner for an iterative inversion scheme, we should investigate the decoupling of the model parameters in terms of the preconditioned migration images. An example for a receiver line with vertical-component data generated by vertical-force sources shows that the density and the Lamé parameters $\lambda + 2\mu$ and μ provide slightly better decoupling than the standard choice of density, P-, and S-impedance.

INTRODUCTION

Migration maps reflections in the recorded data to their correct locations if the given background velocity model is correct. The method correlates the forward wave field generated by a source with the time-reversed or back-propagated wave field generated by the recorded data at the receiver positions. The hessian plays an important role in the migration scheme because it corrects for acquisition imprint and geometrical spreading. Mathematically, the hessian contains the second derivatives of the least-squares error functional with respect to the model parameters. The error is the difference between modeled and observed data. The gradient or derivative with respect to the model parameters determines the direction in which the model should be updated. The gradient is equivalent to a migration image (Lailly, 1983; Tarantola, 1984). Multiplying the gradient with the inverse of hessian determines an optimal step towards the minimum. Computationally, the hessian is out of reach for large-scale applications, although it is sometimes used for smaller-size problems (Pratt et al., 1998; Houten et al., 1999). However, a suitable diagonal approximation is already sufficient for the linearized acoustic case, as shown by Plessix and Mulder (2004) who mix results from the gradient computation with analytical estimates. Gélis et al. (2007) compute the diagonal of the hessian without approximations for the elastic case. Physically, the hessian can be interpreted as the migration image obtained from reflection data generated by a delta-function perturbation of one of the model parameters. For that reason, several authors (von Seggern, 1991; Wapenaar, 1997; Berkhout et al., 2001; Chen and Schuster, 1999; Toxopeus et al., 2004) use the term resolution function. Ideally, the resulting image reproduces the original point-like perturbation. In practice, artifacts occur because of the finite length of the receiver array, the finite number of shots, and the finite band-width of the recorded data. A vertical-force source generates P- and SV-waves. The scatterer also produces both P- and SV-waves. Migration of, for instance, the recorded vertical component will mix these wave types and generate artifacts. Stacking the migration results of many shots will reduce the amplitude of the artifacts but may not completely remove them. In addition, the perturbation of one of the three elastic model parameters produces images in all three parameters. Therefore, the hessian consists of 3×3 matrix blocks in each point.

Beylkin and Burridge (1987, 1990) showed that the hessian is block-diagonal in the high-frequency asymptotic limit, as used in ray theory, if multi-pathing is avoided. Applying the inverse of the small 3×3 block to migration images for each of the elastic parameters solves the linearized inverse problem. In practice, the inverse can be ill-conditioned. Beydoun and Mendes (1989) used the 3D far-field Green functions for the homogeneous isotropic elastic case and 2D ray tracing for the heterogeneous case. Jin et al. (1992) considered iterative elastic inversion in the 2D ray-based case and employed a block-diagonal approximation of the hessian. The authors determined the condition number of these small matrices to assess the well-posedness of the inverse problem. Eigenvalue analysis or singular-value decomposition as a function of reflection angle provides more detailed information about well-posedness. P-P scattering was considered by de Nicolao et al. (1993). Lebrun et al. (2001) included P-S, S-P, and S-S reflections. Bostock and Rondenay (1999) applied these ideas to seismological problems. Tura and Johnson (1993) lists the scattered field for the homogeneous isotropic case with a point scatterer. They describe ways to invert for the parameters of the scatterer in a stable manner. Eaton and Stewart (1994) and Burridge et al. (1998) treated the anisotropic elastic case in the high-frequency asymptotic regime.

Here, we revisit the hessian for the homogeneous isotropic elastic case. Our motivation is a frequency-domain elastic inversion code that generalizes the acoustic work by Pratt (1999), Plessix and Mulder (2004), Mulder and Plessix (2004), and many others. A suitable approximate hessian will improve the efficiency of an elastic migration code. We limit ourselves to the case of a vertical-force source and vertical-component data. The choice of model parameters affects the amplitudes of the main- and off-diagonals of the hessian. Tarantola (1986) showed that a representation in density, P-, and S-impedance is a good choice. Another issue is how well multiplication by the inverse of the block-diagonal part of the hessian affects the decoupling of model parameters and amplitudes of artifacts.

RESULTS

The equations for the 3D scattered field due to a point scatterer in a homogeneous background can be found in, for instance, the paper by Wu and Aki (1985). The scattered field can be constructed from the Green functions (Aki and Richards, 1980; Červený, 2001) and their derivatives. Migration involves similar expressions.

We consider a line of shots between -887.5 and 887.5 m at a 25-m interval at zero depth. The receivers have positions between -900 and 900 m on the same line and with the same interval. We use vertical-force sources and a Ricker wavelet with a peak frequency of 10 Hz. The sources, receivers, and point scatterer are all located in the plane at $y = 0$ m. This means that only P- and SV-waves are involved and no SH-waves. The homogeneous background medium has a density of 2 g/m^3, a P-wave velocity of 2 km/s, and an S-wave velocity of 1.2 km/s. The scattering point is located at $x = 0$ m and a depth given by $z = 750$ m. We computed the hessian in the frequency domain for each shot and all receivers, transformed to the time domain using the Ricker wavelet, and stacked over all shots. Figure 1 displays the hessian for the first, left-most shot and the full line of receivers. The first column of the figure shows the migration result for a point-like perturbation of the density ρ, and the rows display the effect on, subsequently, ρ and the Lamé parameters $\lambda = \rho(v_p^2 - 2v_s^2)$ and $\mu = \rho v_s^2$. Here v_p and v_s are the P- and S-wave velocities, respectively. The second column corresponds to a perturbation of λ and the third of μ. The cleanest image is obtained for the λ-image of a λ-perturbation,

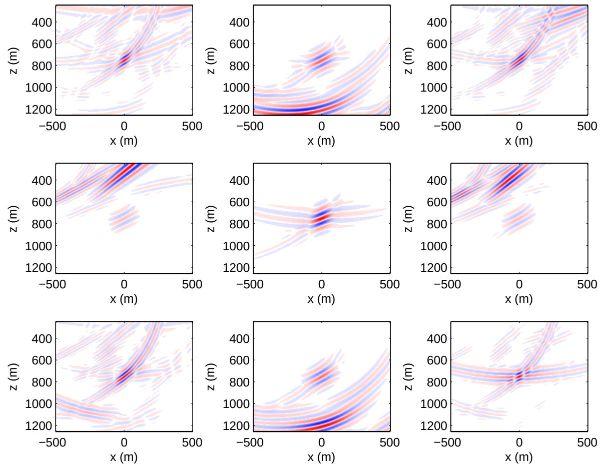

Figure 1: Migration images for a point-scatterer with a single source acting as a vertical force and a line of receivers that recorded the vertical displacement. Depth is on the vertical axis, offset on the horizontal axis. From top to bottom and left to right, the model parameters are $\delta\rho/\rho$, $\delta\lambda/\lambda$, and $\delta\mu/\mu$. The columns from left to right correspond to point-like perturbations of $\delta\rho$, $\delta\lambda$, and $\delta\mu$, respectively. The rows from top to bottom show the migration images for the same parameters.

the central image in Fig. 1. In this case, the artifacts are due to the finite length of the receiver array. In all other cases, we see artifacts caused by incorrect imaging of PP-, PS-, SP-, and SS-scattering. If a PP-scattered wave is imaged as an SS-wave, it produces an artifact at shallower depths than that of the scatterer. Similar artifacts will occur for PS-waves. Note that SS-scattering produces the sharpest results because S-waves have the shortest wavelengths. They produce the larger amplitudes for the same reason.

Ideally, the hessian consists of spikes at the scattering point and the model parameters decouple, that is, a perturbation of one parameter does not produce an image in the other. In other words, we want all off-diagonal migration images to be zero everywhere. Stacking all

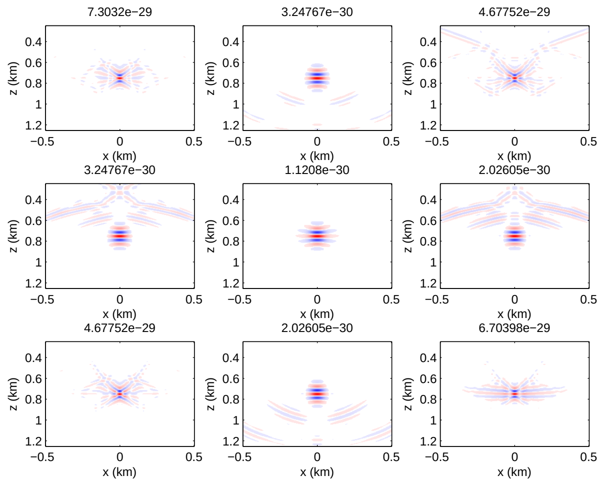

Figure 2: The images after stacking the results for all sources. The number at the top of each panel represents the maximum amplitude.

sources produces the result shown in Fig. 2. Compared to Fig. 1, the summation reduces the amplitudes of the artifacts but does not remove the interaction between model parameters. The $\delta\lambda/\lambda$-image caused by a perturbation of the same parameter, is shown in the central panel of Fig. 2. It has a relatively small amplitude compared to the $\delta\lambda/\lambda$-images caused by a perturbations in one of the other parameters. Using $\lambda+2\mu$ instead of λ improves the situation, as displayed in Fig. 3. We may ask if there exists a set of three model parameters that further boosts the images on the diagonal and reduces the amplitudes of the off-diagonal images. A more common parameter choice consists of density ρ, P-impedance ρv_p, and S-impedance ρv_s (Tarantola, 1986). Figure 4 shows the result for this model representation based on all sources and receivers. There are no strong events besides the ones at the location of the scatterer. The ratio of the maximum values on the diagonal and off-diagonal maximum values is also better than in the case of the Lamé parameters. However, the S-impedance perturbation produces a large correction in the $\delta\rho/\rho$-image, roughly of the same size as the image generated by the $\delta\rho/\rho$-perturbation.

Up to this point, we have only considered the hessian to assess the quality of the migration image. We now want to assess its rôle in parameter updating. With an elastic inversion code in mind, we would like to use the inverse of the block-diagonal part of the hessian as a preconditioner for the inversion – or at least some cost-effective approximation of its block-diagonal. To get an indication of its behavior, we have not computed this 3×3 block in each subsurface point, but only at the scatterer and applied its inverse to the images in Fig. 4. The condition number, the ratio of the largest to the smallest eigenvalue, of the 3×3 matrix was 7.4. Figure 5 displays the result. The maximum amplitude of the images on the diagonal is now 1, as it should. However, the amplitude of one of the off-diagonal images, the effect of a scaled S-impedance perturbation, $\delta(\rho v_s)/(\rho v_s)$, on the scaled density, $\delta\rho/\rho$, is larger than 1, showing that the S-impedance and density are not decoupled very well. We repeated this exercise for a model representation in $\delta\rho/\rho$, $\delta\lambda/\lambda$, and $\delta\mu/\mu$, but this also produced off-diagonal images with an amplitude larger than one. On top of that, the small 3×3 matrix had a rather poor condition number of 120. However, for a representation in $\delta\rho/\rho$, $\delta(\lambda+2\mu)/(\lambda+2\mu)$, and $\delta\mu/\mu$, we obtained the results displayed in Fig. 6. The condition number of the small 3×3 matrix was 11.9, so not as good as for the previous case, but not too bad either. Now, the images on the diagonal have the largest amplitude, although not much larger than most of the off-diagonal images. Nevertheless, this choice of parameters is not worse than the usual representation in terms of density and impedances. Also, it is more natural from an implementation point of view, as the elastic equations are homogeneous of degree one in ρ, $\lambda+\gamma\mu$, and μ, γ being an arbitrary constant which is typically chosen as 0, $2/3$, or 2.

CONCLUSIONS

Several authors have studied the hessian in the context of linearized elastic inversion. The classic choice of density, P-, and S-impedance for the representation of the elastic parameters produces a reasonable decoupling when imaging vertical-component data produced by vertical-force sources. When the migration image is preconditioned by the block diagonal of the hessian, however, density, $\lambda+2\mu$ and μ provide slightly better results. Here, we only considered the vertical data component. We still want to investigate the inclusion of other data components and force-source directions, as well as other model representations.

ACKNOWLEDGEMENTS

This work is part of the research programme of the 'Stichting voor Fundamenteel Onderzoek der Materie (FOM)', which is financially supported by the 'Nederlandse Organisatie voor Wetenschappelijk Onderzoek' (NWO).

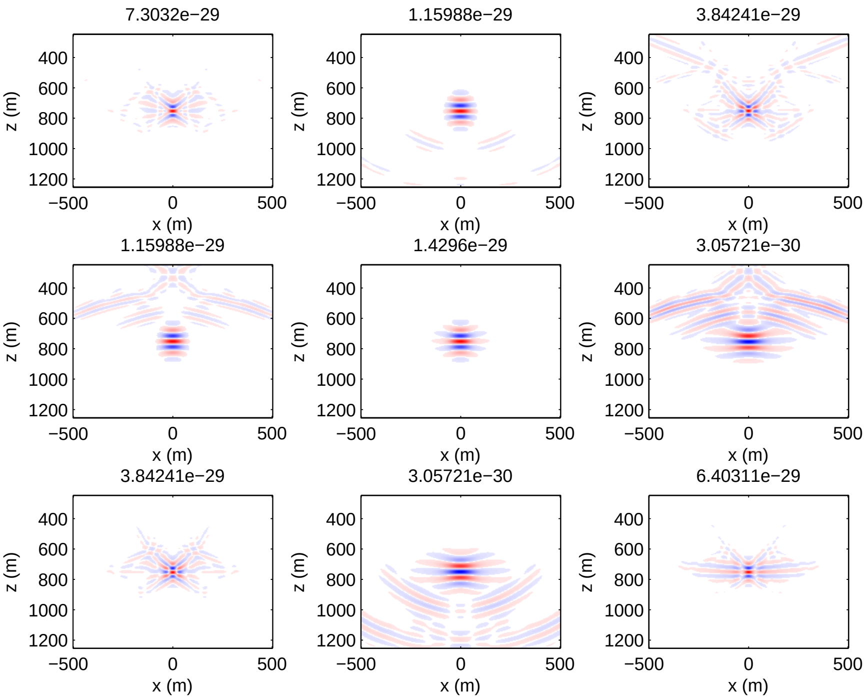

Figure 3: Images after stacking the full survey using $\lambda + 2\mu$ instead of λ. The columns from left to right correspond to point-like perturbations of $\delta\rho/\rho$, $\delta(\rho v_p^2)/(\rho v_p^2)$, and $\delta(\rho v_s^2)/(\rho v_s^2)$, respectively. The rows from top to bottom show the migration images for the same parameters. The number at the top of each panel represents the maximum amplitude.

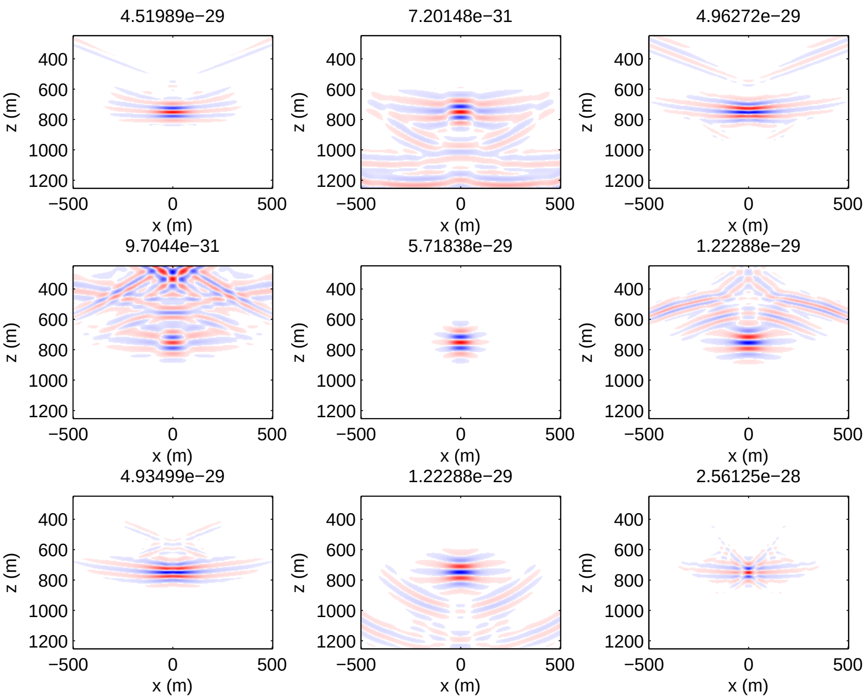

Figure 4: Migration image for a point-scatterer for a line of vertical-force sources and vertical-component receivers. The columns from left to right correspond to point-like perturbations of $\delta\rho/\rho$, $\delta(\rho v_p)/(\rho v_p)$, and $\delta(\rho v_s)/(\rho v_s)$, respectively. The rows from top to bottom show the migration images for the same parameters. The number at the top of each panel represents the maximum amplitude.

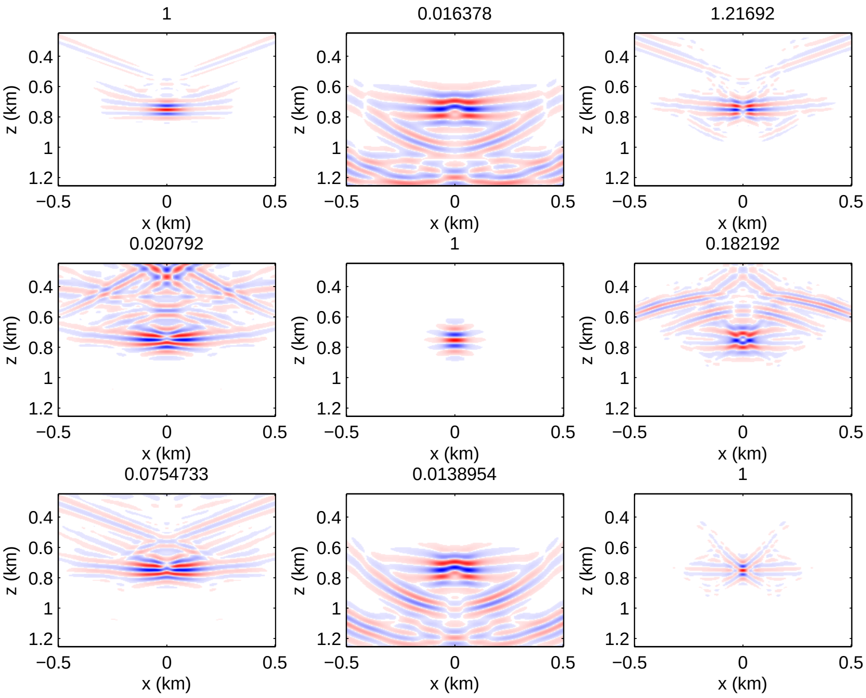

Figure 5: As Fig. 4, but now left-multiplied by the inverse of the diagonal block of the hessian at the scatterer. The columns from left to right correspond to point-like perturbations of $\delta\rho/\rho$, $\delta(\rho v_p)/(\rho v_p)$, and $\delta(\rho v_s)/(\rho v_s)$, respectively.

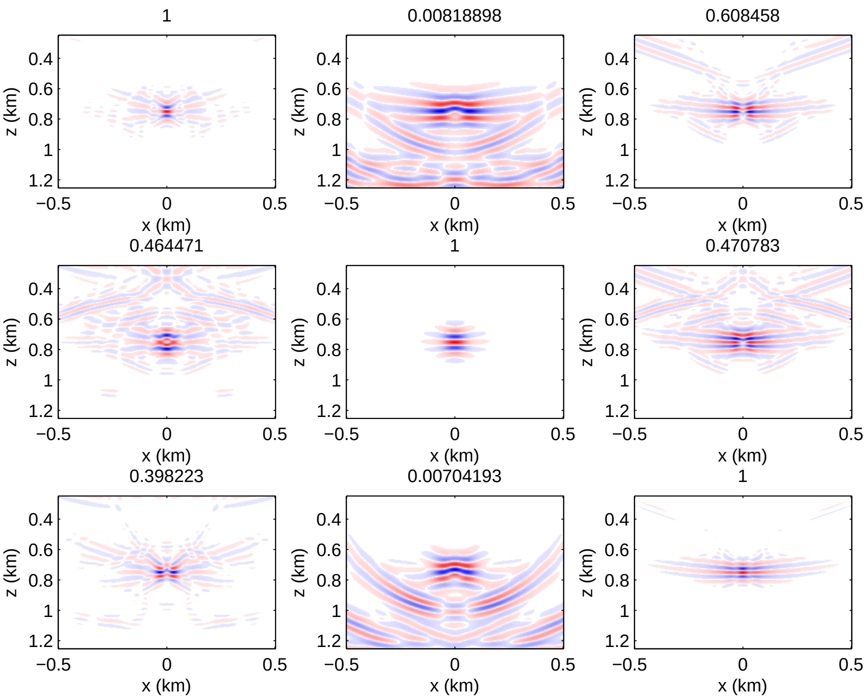

Figure 6: As Fig. 5, but now for model parameters $\{\delta\rho/\rho, \delta(\lambda+2\mu)/(\lambda+2\mu), \delta\mu/\mu\}$.

EDITED REFERENCES

Note: This reference list is a copy-edited version of the reference list submitted by the author. Reference lists for the 2007 SEG Technical Program Expanded Abstracts have been copy edited so that references provided with the online metadata for each paper will achieve a high degree of linking to cited sources that appear on the Web.

REFERENCES

Aki, K., and P. G. Richards, 1980, Quantitative seismology: W. H. Freeman and Company.

Berkhout, A. J., L. Ongkiehong, A. W. F. Volker, and G. Blacquiere, 2001, Comprehensive assessment of seismic acquisition geometries by focal beams - Part I: Theoretical considerations: Geophysics, 66, 911–917.

Beydoun, W., and M. Mendes, 1989, Elastic ray-born l2-migration/inversion: Geophysical Journal International, 97, 151– 160.

Beylkin, G., and R. Burridge, 1987, Multiparameter inversion for acoustic and elastic media: 57th Annual International Meeting, SEG, Expanded Abstracts, 6, 747–749.

———, 1990, Linearized inverse scattering problems in acoustics and elasticity: Wave Motion, 12, 15–52.

Bostock, M. G., and S. Rondenay, 1999, Migration of scattered teleseismic body waves: Geophysical Journal International, 137, 732–746.

Burridge, R., M. V. de Hoop, D. Miller, and C. Spencer, 1998, Multiparameter inversion in anisotropic elastic media: Geophysical Journal International, 134, 757–777.

Cerveny, V., 2001, Seismic ray theory: Cambridge University Press.

Chen, J., and G. T. Schuster, 1999, Resolution limits of migrated images: Geophysics, 64, 1046–1053.

de Nicolao, A., G. Drufuca, and F. Rocca, 1993, Eigenvalues and eigenvectors of linearized elastic inversion: Geophysics, 58, 670–679.

Eaton, D. W. S., and R. R. Stewart, 1994, Migration/inversion for transversely isotropic elastic media: Geophysical Journal International, 119, 667–683.

Gelis, C., J. Virieux, and G. Grandjean, 2007, Two-dimensional elastic full waveform inversion using Born and Rytov formulations in the frequency domain: Geophysical Journal International, 168, 605–633.

Houten, E. E. W. V., K. D. Paulsen, M. I. Miga, F. E. Kennedy, and J. B. Weaver, 1999, An overlapping subzone technique for MR-based elastic property reconstruction: Magnetic Resonance in Medicine, 2, 779–786.

Jin, S., R. Madariaga, J. Virieux, and G. Lambaré, 1992, Two-dimensional asymptotic iterative elastic inversion: Geophysical Journal International, 108, 575–588.

Lailly, P., 1983, The seismic inverse problem as a sequence of before stack migration: Proceedings of the Conference on Inverse Scattering: Theory and Applications, SIAM, 206–220.

Lebrun, D., V. Richard, D. Mace, and M. Cuer, 2001, SVD for multioffset linearized inversion: Resolution analysis in multicomponent acquisition: Geophysics, 66, 871–882.

Mulder, W. A., and R.-E. Plessix, 2004, A comparison between one-way and two-way wave-equation migration: Geophysics, 69, 1491–1504.

Plessix, R. -E., and W. A. Mulder, 2004, Frequency-domain finite difference amplitude-preserving migration: Geophysical Journal International, 157, 975–987.

Pratt, R. G., 1999, Seismic waveform inversion in the frequency domain, part 1: Theory and verification in a physical scale model: Geophysics, 64, 888–901.

Pratt, R. G., C. S. Shin, and G. J. Hicks, 1998, Gauss-Newton and full Newton methods in frequency-space seismic waveform inversion: Geophysical Journal International, 133, 341–362.

Tarantola, A., 1984, Inversion of seismic reflection data in the acoustic approximation: Geophysics, 49, 1259–1266.

———, 1986, A strategy for nonlinear elastic inversion of seismic reflection data: Geophysics, 51, 1893–1903.

Toxopeus, G., S. Petersen, J. Thorbecke, and K. Wapenaar, 2004, Simulating high resolution inversion: Decomposing the resolution function: 74th Annual International Meeting, SEG, Expanded Abstracts, 1798–1801.

Tura, M. A. C., and L. R. Johnson, 1993, A stable method for linearized inversion of elastic parameters: Geophysical Journal International, 115, 1–13.

von Seggern, D., 1991, Spatial resolution of acoustic imaging with the Born approximation: Geophysics, 56, 1185–1202.

Wapenaar, C. P. A., 1997, 3-D migration of cross-spread data: Resolution and amplitude aspects: Geophysics, 62, 1220–1225.

Wu, R., and K. Aki, 1985, Scattering characteristics of elastic waves by an elastic heterogeneity: Geophysics, 50, 582–595.